

Advances in Automated Error Assessment of Spherical Near-Field Antenna Measurements

Patrick Pelland, Greg Hindman, Allen Newell
Nearfield Systems Inc.
19730 Magellan Drive,
Torrance, CA 90502-1104

Abstract — Over the years, spherical near-field (SNF) antenna measurements have become increasingly popular for characterizing a wide variety of antenna types. The SNF configuration allows one to measure data over a sphere surrounding the antenna, which provides it a unique advantage over planar and cylindrical near-field systems where measurement truncation is inherent. Like all antenna measurement configurations, SNF systems are susceptible to a number of measurement errors that, if not properly understood, can corrupt the antenna's far-field parameters of interest (directivity, beamwidth, beam pointing, etc.). The NIST 18-term error assessment originally developed for planar near-field measurements [1] has been adapted for SNF systems [2] and provides an accurate measure of the uncertainty in a particular SNF measurement. Once particular measurement errors are known, steps can be taken to reduce their impact on far-field radiation patterns. When manually assessing all 18 terms of the NIST uncertainty budget this procedure becomes tedious and time consuming.

This paper will describe an acquisition algorithm that allows one to analyze all 18 error terms or a subset of those in automated fashion with minimal user intervention. Building upon previous research toward developing an automated SNF error assessment algorithm [3, 4], this new procedure will automatically generate tabulated and plotted uncertainty data for directivity, beamwidth and beam pointing of a particular far-field radiation pattern. Once measurement uncertainties are known, various post-processing techniques can be applied to improve far-field radiation patterns. Results will be shown for three antennas measured on large phi-over-theta SNF scanners.

Index Terms—NIST, 18-term, Error Evaluation, Spherical Near-Field, Measurement Automation, Analysis, Uncertainty.

I. INTRODUCTION

In [3] the authors described a measurement procedure that would enable one to perform an assessment of spherical near-field (SNF) measurement errors based on a set of practical tests that can be performed in any SNF facility. The purpose was to enable a typical SNF system to provide error bars for the measured radiation patterns in an automated fashion. A specific set of measurements that could be used to assess all significant sources of error in SNF measurements was identified. This set of tests was designed to minimize chamber occupancy time while still providing an accurate measure of the uncertainty in a particular SNF set up. The standard NIST 18-term error budget originally developed for planar near-field

facilities [1] was used as a starting point with some adaptations for SNF systems found in [2].

Reference [4] expanded on the research by outlining some specific implementation details of the automated error assessment scheme. In particular, results of the procedure were presented for various antenna types and operating frequencies. Some additional details about the required measurements and comparison techniques were also presented to the reader.

This paper will describe the most recent advancements in the automation of SNF measurement error assessment and some additional implementation details. Section II will summarize the fundamentals of the automated error assessment procedure through reference to past literature to make the most efficient use of the space available here. Next, in Section III the reader will be presented with a selection of antenna types used to validate this automated process on spherical near-field test systems. In Section IV, outcomes of the error analysis of some of the specific error terms will be presented and discussed along with some post-processing techniques used. Section V will show the user some final outcomes of the automated procedure, including tabulated error budgets and radiation patterns showing error bounds. Finally, some conclusions will be drawn in Section VI and some proposed future work will also be outlined.

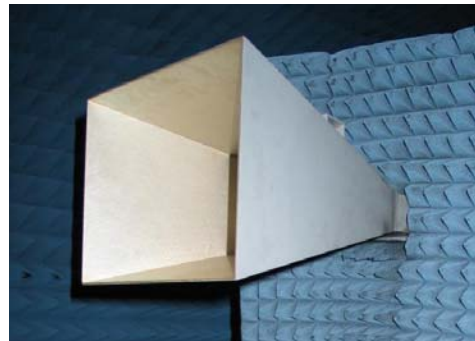


Figure 1. Pyramidal Horn Antenna (EMCO 3160-03 Standard Gain Horn).

II. BASICS OF THE AUTOMATED ERROR ASSESSMENT PROCEDURE

The procedure for the acquisition of all required measurements and analysis of the 18 sources of uncertainty has not changed significantly since [3] and [4] so the reader is

encouraged to become familiar with both. The sources of error are organized into 18 terms as outlined in [3, Table I] and [3, Table II]. A total of six SNF measurements is required to perform the assessment on a particular antenna under test (AUT) as outlined in [4, Table 1] with some relevant terminology explained in [4, Table 2]. From this set of near-field tests, along with some known data that need be determined only once for a given SNF facility and not for every AUT tested, the contribution of each term in the modified NIST budget of [3, Table I] and [3, Table II] may be estimated. These error contributions are then combined in a root-sum-of-squares fashion in order to obtain the overall measurement uncertainty at each pattern angle over the entire radiation sphere surrounding the AUT. This procedure can also be used to provide an estimate of total uncertainty in various other far-field parameters of interest, including directivity, peak gain, beamwidth and beam pointing direction.

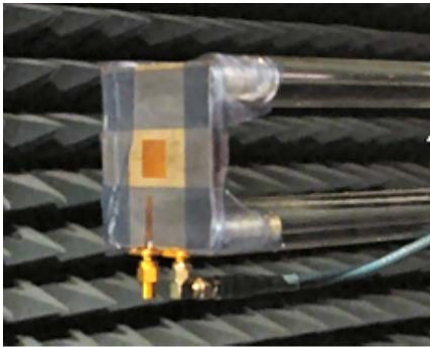


Figure 2. Low Gain Patch Antenna Mounted on an SNF Scanner.

III. AUT TYPES AND OPERATING FREQUENCIES

The three AUTs discussed in this paper will be described in this section. Some results for two of the three antennas described here were also considered in [4] with new data being presented for both in the present paper. The first AUT is the pyramidal horn antenna shown in Figure 1. This medium gain AUT is used at L-band frequencies as a gain reference antenna. Next, the microstrip patch antenna shown in Figure 2 was chosen because it operates in a different frequency band and has much lower gain than the other antennas tested. Finally, the X-band slotted waveguide array shown in Figure 3 was selected for analysis because of its operating frequency and much higher gain than the other two antennas.



Figure 3. X-Band Slotted Waveguide Array

IV. OUTCOMES OF THE ERROR ASSESSMENT FOR SELECTED ERROR TERMS

Three of the eighteen error terms have been selected for closer examination. The techniques used to assess the impact of these terms will next be discussed in turn.

A. Error Term #8: Data Point Spacing

This term relates to far-field errors introduced by the finite number of sample points used in the near-field measurement. The concept has ties to the well-known Nyquist sampling theorem, in that constructing far-field patterns from near-field data requires that the sampling points be spaced at a minimum of a half wavelength on the surface of the minimum sphere. Theoretically, this sampling density should ensure that the highest spatial frequency components will be captured by the near-field measurement. However, other factors can create the need for denser near-field sampling [5].

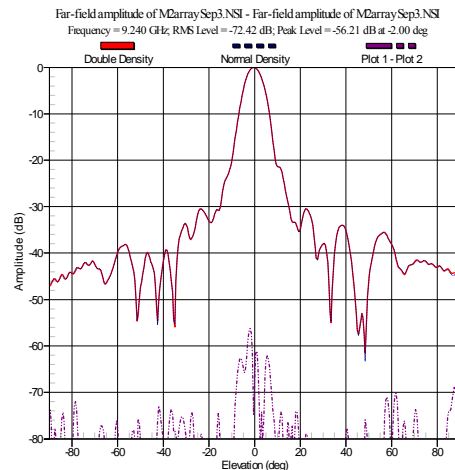


Figure 4. Error Term #8 Results for the X-Band Slotted Waveguide Array

In order to validate that the typical $\lambda/2$ sampling density is sufficient to properly characterize the performance of the AUT the technique chosen here is to acquire near-field data at a higher sampling density and compare to the normal sampling density. In the interest of automating the analysis of this error term, a single $\lambda/4$ -sampled measurement is acquired on the SNF system. Next, the regular density ($\lambda/2$) subset of that near-field data is automatically extracted and the resulting far-field pattern is compared to the $\lambda/4$ -sampled far-field pattern. This technique should provide a reasonable estimate of the uncertainty associated with data point spacing. Making use of a single measurement also helps isolate the analysis of this error term from the effects of random errors and decreases overall measurement time. If the resulting difference between the two patterns (the equivalent stray signal [9]) shows large variations then the baseline sampling density should be increased. Figure 4 shows the results of this analysis technique for the H-plane pattern cut of the slotted waveguide array antenna using the NSI-developed “Plot Subtraction” software [9]. After performing a complex subtraction on the $\lambda/4$ -sampled case (—) and the extracted $\lambda/2$ -subset of that data (---) the resulting error level is shown (---). Since the difference level

is sufficiently low this technique helped validate the baseline $\lambda/2$ sampling density.

B. Error Term #14: Systematic Phase Errors

This error term addresses all phase errors introduced by the receiving system, including but not limited to receiver errors, cable flexing, rotary joint transmission variations and thermal drift over the course of the measurement. For a spherical near-field test system that contains RF rotary joints and no flexing cables, the two most significant contributors to this error term are thermal drift and the undesired amplitude and phase variations as a function of angle introduced by the system's rotary joints. This automated procedure is capable of analyzing and reducing the effects of these sources of error using two unique post-processing techniques developed by NSI.

Thermal drift during measurements can cause changes in the RF properties of the system's transmission lines, electronic components and the apparent beam peak location of the AUT. These can be corrected by periodically returning to a reference point on the measurement grid and recording amplitude and phase as described in the NSI developed MTI technique, recently adapted for use on SNF test systems. Numerical correction is then applied to the measured data [6] to reduce the effects of thermal drift on the resulting far-field radiation parameters.

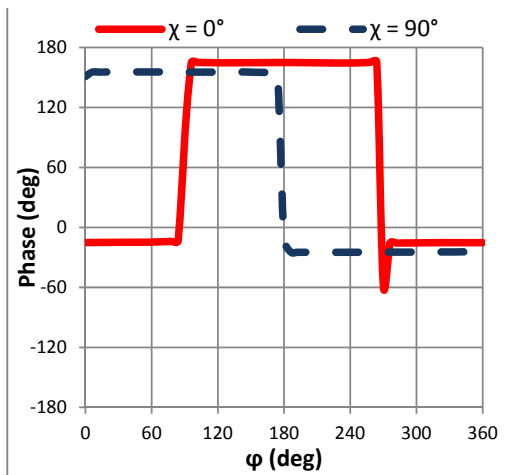


Figure 5. Near-field $\theta = 0^\circ$ Polarization Cuts showing 8.59° Phase Imbalance between $\chi = 0^\circ$ and $\chi = 90^\circ$

The authors of [4] identify a useful test for estimating the near-field variations as a function of rotary joint position by rotating both the AUT and probe in unison and recording amplitude and phase at all positions. While this test can shed some light on the effects of systematic phase errors, the results will also be affected by range misalignment and room scattering. Furthermore, this technique can be useful for error analysis but cannot be used for post-processing field corrections. An alternative approach is to make use of a multi-point channel-balance (MPCB) correction scheme similar to that presented in [7], where the on-axis ($\theta = 0^\circ$) fields for $\chi = 0^\circ, 90^\circ$ as a function of ϕ are compared and corrected. The MPCB technique relies on the fact that at $\theta = 0^\circ$ the two ϕ cuts

should radiate identical fields rotated by 90° . After de-rotation the fields can be compared and adjusted.

For the purposes of this automation process, a five-point MPCB correction procedure has been implemented by NSI. The amplitudes and phases of the two polarization components are compared at $(\theta, \phi) = (0, 0), (0, 90), (0, 180), (0, 270), (0, 360)$ and correction is applied as outlined in [5].

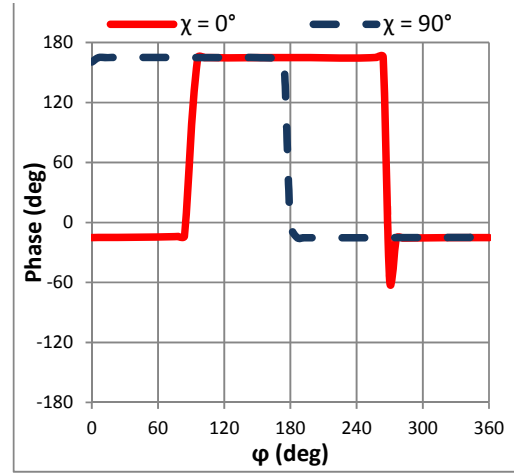


Figure 6. Near-field $\theta = 0^\circ$ Polarization Cuts after 8.59° Correction Applied to $\chi = 90^\circ$ Data

Figure 5 shows the two uncorrected $\theta = 0^\circ$ phase cuts used for the MPCB correction algorithm of the automated procedure for the L-band horn. After performing a phase adjustment of 8.59° on the $\chi = 90^\circ$ data (---), the rotational phase variations have been artificially reduced as illustrated in Figure 6. While it is not shown here, an amplitude adjustment of roughly 0.3 dB was also applied to the near-field data. The resulting far-field patterns of the uncorrected and corrected cases are shown in Figure 7. The results of this error assessment led to the eventual replacement of the rotary joint since its rotational RF variations were affecting the main beam of the antenna's radiation pattern severely, as shown by the large difference (---) between the uncorrected (—) and corrected (---) plots of Figure 7. After replacing the χ -axis rotary joint the uncorrected vs. MPCB data has been greatly improved as shown in Figure 8.

C. Error Term #16: Room Scattering

The authors of [2, 4] suggest using two different sampling strategies for comparison to estimate the effects of room scattering on a far-field radiation pattern. Since these two measurement geometries will have reflection contributions from different parts of the chamber, a comparison of the two should yield an ample upper bound to the error associated with this term. While this method can provide a conservative estimate of the scattering level in the range, it has limited use as a post-processing correction technique.

A more elegant approach is to make use of a reflection suppression algorithm like the NSI developed "Mathematical Absorber Reflection Suppression" (MARS) technique [8]. With proper care during the measurement setup phase this technique has been shown to compute and suppress the effects

of chamber scattering to a high degree of accuracy. This technique makes no assumptions about the radiation properties of the AUT so it is ideally suited for automation.

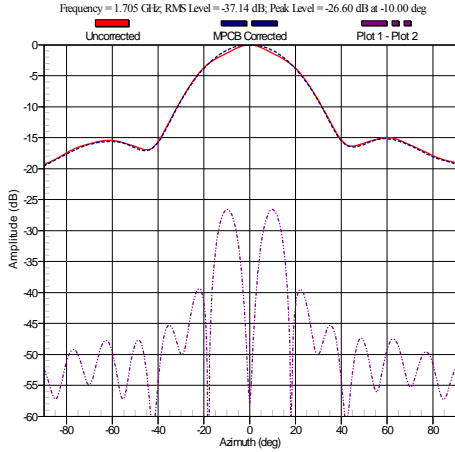


Figure 7. Error Term #14 Results for the L-Band Horn AUT with a Marginally Performing Rotary Joint which was Subsequently Replaced

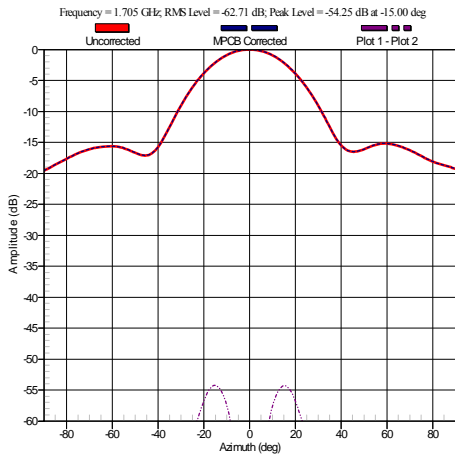


Figure 8. Figure Error Term #14 Results for the L-Band Horn AUT After Replacement of the χ -axis Rotary Joint

V. PRESENTING FINAL UNCERTAINTY BUDGETS

Once all required measurements, analysis and data corrections have been completed, the results of the automated error assessment must be presented to the end-user in a meaningful format. Uncertainty budgets are typically desired for a variety of far-field parameters including but not limited to gain, sidelobes, beam pointing direction, cross-pol and axial ratio. Table I shows the gain uncertainty budget compiled by the automated procedure for the X-band slotted waveguide array shown in Figure 3. This table compiles the results of the error analysis techniques for each error term and performs a root-sum-of-squares addition to estimate the overall peak gain uncertainty. While a tabulated uncertainty budget is ideally suited for outlining the most significant contributors to gain uncertainty, there are times when radiation patterns showing upper and lower bounds due to total uncertainty are desired.

TABLE I. GAIN UNCERTAINTY BUDGET FOR X-BAND THE SLOTTED WAVEGUIDE ARRAY

Gain Budget Error Term	Uncertainty
1. Probe Relative Pattern	0.00 dB
2. Probe Polarization ($p' = 20$ dB)	0.00 dB
3. Calibrated Probe Gain	0.15 dB
4. Probe Alignment	0.00 dB
5. Normalization Constant	0.16 dB
6. AUT/SGH Impedance Mismatch	0.06 dB
7. AUT Alignment	N/A
8. Data Point Spacing	0.02 dB
9. Data Truncation	N/A
10. Sphere Radius Errors	0.00 dB
11. Sphere Theta/Phi Errors	0.01 dB
12. Higher Order Coupling	0.03 dB
13. Receiver Amplitude Non-Linearity	0.00 dB
14. System Phase Errors	0.03 dB
15. Receiver Dynamic Range	0.00 dB
16. Room Scattering	0.01 dB
17. Cable Leakage	0.00 dB
18. Repeatability and Random Errors	0.00 dB
Gain Total Uncertainty (RSS)	0.23 dB

In order to validate the results of the procedure, the low gain microstrip patch antenna shown in Figure 2 was installed by an inexperienced range operator and the error assessment was automated. Figure 9 shows the resulting E-plane amplitude pattern cut plotted with the upper and lower bounds due to total uncertainty after analysis was completed for every term with no corrections applied. High levels of chamber scattering, poor system alignment, low signal-to-noise, minimal absorber treatment and other sources of error have led to very high uncertainty at the edges of the pattern. After the software has automatically performed several post-processing techniques (MARS, MTI, MPCB correction and θ/ϕ non-intersection correction) the resulting far-field radiation pattern uncertainty has been drastically reduced as shown in Figure 10.

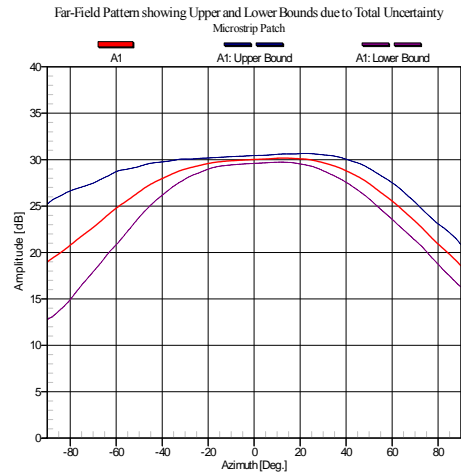


Figure 9. Far-Field Radiation Pattern for the Microstrip Patch (—) showing Upper (—) and Lower (—) due to Total Uncertainty

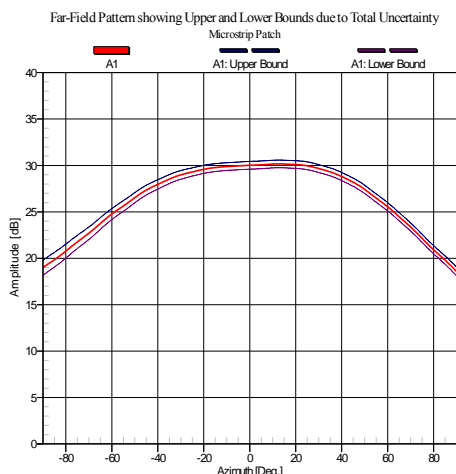


Figure 10. Far-Field Radiation Pattern for the Microstrip Patch (—) showing Upper (---) and Lower (---) due to Total Uncertainty after Performing Various Post-Processing Corrections

Figure 11 shows a similar E-plane pattern cut for the X-band waveguide array without any post-processing corrections applied. Based on the gain uncertainty budget presented in Table I and the pattern cut shown in Figure 10, it was decided that measurement uncertainties were within acceptable limits, in contrast with the results for the low gain patch before corrections were applied. Finally, Table II shows a -15 dB sidelobe uncertainty budget automatically compiled by the error assessment software for the L-band horn shown in Figure 1. These results were compiled after the malfunctioning rotary joint previously discussed was replaced with a new, phase stable unit. Error terms #3, #5 and #6 are omitted since they affect overall peak gain uncertainty only.

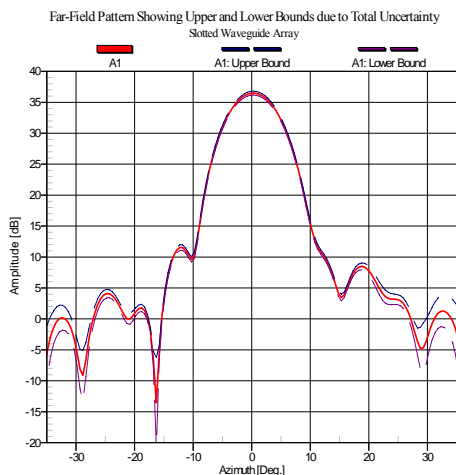


Figure 11. Far-Field Radiation Pattern for the X-band Array (—) showing Upper (---) and Lower (---) due to Total Uncertainty

VI. CONCLUDING REMARKS

This paper expands on previous research by improving and optimizing an existing automated error assessment procedure

for spherical near-field antenna test systems. The process allows one to assess the uncertainty of various far-field radiation parameters based on the NIST 18-term error budget in an automated sense with minimal user intervention. Once the error analysis phase has been completed, the software also performs various post-processing correction algorithms based on techniques developed by NSI for spherical near-field antenna measurements. Total uncertainty is automatically presented to the user in a variety of formats of which several were shown here.

TABLE II. -15 dB SIDELobe UNCERTAINTY BUDGET FOR THE L-BAND STANDARD GAIN HORN

-15 dB Sidelobe Uncertainty Budget	Uncertainty
1. Probe Relative Pattern	0.00 dB
2. Probe Polarization	0.02 dB
4. Probe Alignment	0.00 dB
7. AUT Alignment	N/A
8. Data Point Spacing	0.16 dB
9. Data Truncation	N/A
10. Sphere Radius Errors	0.01 dB
11. Sphere Theta/Phi Errors	0.40 dB
12. Higher Order Coupling	0.40 dB
13. Receiver Amplitude Non-Linearity	0.00 dB
14. System Phase Errors	0.08 dB
15. Receiver Dynamic Range	0.00 dB
16. Room Scattering	0.64 dB
17. Cable Leakage	0.00 dB
18. Repeatability and Random Errors	0.05 dB
Pattern Sidelobe Uncertainty (RSS)	0.87 dB

REFERENCES

- [1] A. Newell, "Error Analysis Techniques for Planar Near-Field Measurements", IEEE Trans Antennas & Propagation, AP-36, p. 581, 1988.
- [2] G. Hindman, A. Newell, "Simplified Near-Field Accuracy Assessment", Proc. Antenna Measurement Techniques Association (AMTA) Annual Symp., 2006.
- [3] P. Pelland, J. Ethier, D. J. Janse van Rensburg, D. A. McNamara, L. Shafai & S. Mishra, "Towards Routine Automated Error Assessment in Antenna Spherical Near-field Measurements", Proc. 4th European Conf. Antennas & Propagation (EuCAP 2012), April 2010.
- [4] P. Pelland, D. J. Janse van Rensburg, D. A. McNamara, L. Shafai, S. Mishra & M. Gavrilovic, "Some Detailed Implementation Aspects of an Automated Error Assessment Scheme for Antenna Spherical Near-Field Measurements", Proc. Antenna Measurement Techniques Association (AMTA) Annual Symp., 2010.
- [5] A. Newell, G. Hindman, "Planar and Spherical Near-Field Range Comparison with -60 dB Residual Error Level", Proc. Antenna Measurement Techniques Association (AMTA) Annual Symp., 2007.
- [6] G. Hindman, D. Slater, "Thermal Error Corrections in Near-Field Measurements", Proc. Antenna Measurement Techniques Association (AMTA) Annual Symp., 1995.
- [7] Gregson S., McCormick J., Parini C., "Principles of Planar Near-Field Antenna Measurements", The Institute of Engineering and Technology, 2007, pp. 198-201.
- [8] G. Hindman, A. Newell, "Mathematical Absorber Reflection Suppression (MARS) for Anechoic Chamber Evaluation and Improvement", Proc. Antenna Measurement Techniques Association (AMTA) Annual Symp., 2008.
- [9] A. Newell, G. Hindman, "Antenna Pattern Comparison Using Pattern Subtraction and Statistical Analysis", Proc. 5th European Conf. Antennas & Propagation (EuCap 2011), April 2011.